Optics Letters

Flat-optics generation of broadband photon pairs with tunable polarization entanglement

VITALIY SULTANOV,[1,2,*] TOMÁS SANTIAGO-CRUZ,[1,2] AND MARIA V. CHEKHOVA[1,2]

[1]Max-Planck Institute for the Science of Light, Staudtstr. 2, 91058 Erlangen, Germany
[2]Friedrich-Alexander Universität Erlangen-Nürnberg, Staudtstr. 7, 91058 Erlangen, Germany
*Corresponding author: vitaliy.sultanov@mpl.mpg.de

Received 9 March 2022; revised 4 June 2022; accepted 7 July 2022; posted 8 July 2022; published 27 July 2022

The concept of "flat optics" is quickly conquering different fields of photonics, but its implementation in quantum optics is still in its infancy. In particular, polarization entanglement, strongly required in quantum photonics, is so far not realized on "flat" platforms. Meanwhile, relaxed phase matching of "flat" nonlinear optical sources enables enormous freedom in tailoring their polarization properties. Here we use this freedom to generate photon pairs with tunable polarization entanglement via spontaneous parametric downconversion (SPDC) in a 400-nm GaP film. By changing the pump polarization, we tune the polarization state of photon pairs from maximally entangled to almost disentangled, which is impossible in a single bulk SPDC source. Polarization entanglement, together with the broadband frequency spectrum, results in an ultranarrow (12 fs) Hong–Ou–Mandel effect and promises extensions to hyperentanglement.

https://doi.org/10.1364/OL.458133

There is a pronounced tendency in photonics toward "flat" optics [1], involving ultrathin films, 2D materials, and metasurfaces. Linear and nonlinear "flat" optical elements are not only compact, integrable, and efficient; they are also multifunctional, promising to replace their bulk counterparts [2]. Quantum optics is also on its way to "flat" platforms [3,4]. The latter are so far mainly used as hosts for single-photon sources [5] and linear converters of quantum light, both in space [6–8] and in polarization [6,9]. Meanwhile, "flat" quantum optics was so far unable to deliver polarization-entangled photons, which are ubiquitous in quantum technologies – both for quantum communications [10] and optical quantum computation [11]. Although photon pairs have been generated in ultrathin films through spontaneous four-wave mixing [12] and spontaneous parametric downconversion (SPDC) [13–15], it is still bulk crystals that provide polarization entanglement for flat platforms [7,9]. This shortcoming hinders the development of "flat" quantum optics.

At the same time, ultrathin platforms provide unprecedented advantages in engineering photon pairs. Being free from the phase matching constraints, they can be fabricated of materials with especially large second-order susceptibility $\hat{\chi}^{(2)}$, to boost the efficiency of pair generation through SPDC. To tune the degree of polarization entanglement of photon pairs, now we use another consequence of relaxed phase matching in ultrathin SPDC sources: they enable several nonlinear interactions (type-0, type-I, type-II) simultaneously, the only restriction being the structure of the $\hat{\chi}^{(2)}$ tensor.

Here, we generate photon pairs in an ultrathin layer of gallium phosphide (GaP) whose $\hat{\chi}^{(2)}$ tensor enables SPDC of different polarization types. We find that these pairs feature nontrivial polarization properties, in particular, polarization entanglement. Further, we show that by choosing the polarization of the pump, we can easily tune the polarization state of the photon pairs from maximally entangled to almost disentangled and, at the same time, maintain the purity of the state. Such performance is impossible with regular linear polarization elements without introducing polarization-dependent losses in the system [9]. Moreover, in combination with the nearly unbounded frequency spectrum of photon pairs emitted from ultrathin materials [14], polarization entanglement results in a remarkably narrow Hong–Ou–Mandel (HOM) dip or peak, depending on the experimental conditions, which we also demonstrate in experiment. Together with the giant time-frequency [13] and position-momentum [16] entanglement, the observed polarization entanglement can be used to create hyperentangled photon pairs on flat platforms.

As a source of photon pairs, we use a 400-nm film of GaP, which is a semiconductor with a zinc blende symmetry. The film is fabricated on a 4-μm layer of SiO_2, which, in turn, is deposited on a 150-μm sapphire substrate. The fabrication procedure is described in Ref. [17]. The non-zero $\hat{\chi}^{(2)}$ components of GaP are $\chi_{xyz} = \chi_{xzy} = \chi_{yzx} = \chi_{yxz} = \chi_{zyx} = \chi_{zxy} \approx 100$ pm/V [17,18]. To exploit these components, the sample is fabricated with its normal at 15° to the [100] crystalline direction [the inset of Fig. 1(a)], so that the pump field, in the general case, has projections on all crystallographic axes x, y, z. The efficiency of SPDC scales as $|\hat{\chi}^{(2)} \cdot \vec{e}_s \cdot \vec{e}_i \cdot \vec{e}_p|^2$, where $\vec{e}_{s,i,p}$ are the unit polarization vectors of the signal, idler, and pump radiation, respectively [19]. Because of the relaxed phase matching condition, all nonzero elements of the $\hat{\chi}^{(2)}$ tensor of GaP contribute to SPDC; in particular, there is emission of pairs for any pump polarization (see Supplement 1 for details).

To generate photon pairs, we pump the GaP nanolayer by a 60-mW continuous-wave laser at 638 nm [Fig. 1(a)], whose linear polarization can be rotated by a half-wave plate (HWP). We focus the pump into the sample with lens L1 (NA=0.05)

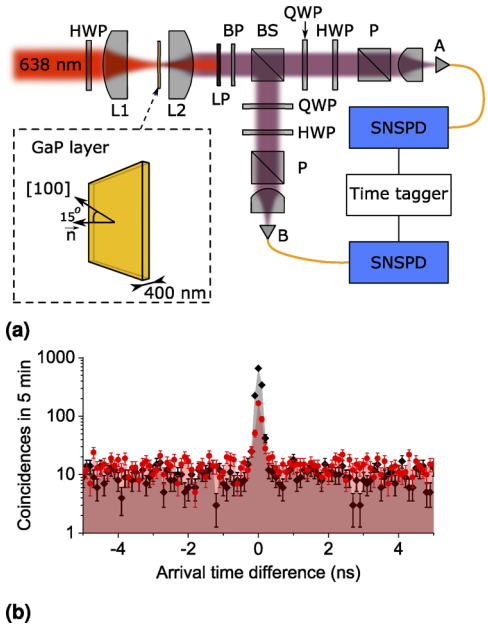

Fig. 1. (a) Continuous-wave pump focused by lens L1 into the GaP film; photon pairs are collected by lens L2 and filtered from the pump by long-pass filters LP and bandpass filter BP. Non-polarizing beam splitter BS sends the photons into arms A and B, each containing a quarter-wave plate (QWP), a half-wave plate (HWP), a polarizer (P), and a superconducting nanowire single-photon detector (SNSPD). A time tagger builds a histogram of arrival time differences. (b) Typical logarithmic-scale histogram for the horizontally (black) and vertically (red) polarized pump.

and collect the generated photon pairs with lens L2 (NA= 0.16). We cut off the pump with four long-pass filters (LP), the cut-on wavelengths being 850 nm for two of them and 1000 nm for the other two. For polarization measurements, we additionally select frequency-degenerate photon pairs with a bandpass filter (BP) centered at 1275 nm with 50-nm full width at half maximum.

After collecting the SPDC radiation and filtering it from the pump, we send it to a Hanbury Brown–Twiss setup [20] formed by non-polarizing beam splitter BS and superconducting nanowire single-photon detectors (SNSPDs) in two output ports A and B. Since the detectors are single-mode, we register collinear photon pairs in a single spatial mode. A time tagger receives photo-detection pulses from both detectors and builds the histogram of their time differences [Fig. 1(b)], where the central peak clearly shows the simultaneity of photon arrivals in both arms. The peak is observed for both vertically (V) and horizontally (H) polarized pumps (red and black points). Events forming this peak, called "two-photon coincidences," indicate the detections of photon pairs. The background of the histogram shows accidental two-photon coincidences, and its level is determined by the product of the two detectors' count rates. The same level of the background despite the significantly different rates of real coincidences (4 Hz and 0.5 Hz for H- and V-polarized pump, respectively) for different pump polarizations shows that accidental coincidences are almost entirely caused by the photoluminescence of the GaP film, which surpasses SPDC, predominantly contributing to single counts (around 19 kHz). In all measurements described below, this background is subtracted.

We see that, in contrast to SPDC in bulk crystals, photon pairs are emitted for both V-polarized and H-polarized pump, although at a higher rate in the latter case [Fig. 1(b)]. Even more strikingly, the two cases result in different polarization states of the photon pairs. A general polarization state of a photon pair in a single frequency and wave vector mode can be written as a qutrit: a superposition of vertically, horizontally, and orthogonally polarized photon pairs [21],

$$|\Psi\rangle = C_1|2\rangle_H|0\rangle_V + C_2|1\rangle_H|1\rangle_V + C_3|0\rangle_H|2\rangle_V, \quad (1)$$

where $|N\rangle_{H,V}$ are the Fock states with N photons polarized horizontally or vertically, respectively, and C_i are the complex amplitudes satisfying $\sum_{i=1}^{3}|C_i|^2 = 1$.

After the beam splitter, the state in Eq. (1) becomes polarization-entangled upon post-selecting the cases where photon pairs are split. The degree of polarization entanglement is given by the concurrence [22,23]:

$$C = \left|2C_1C_3 - C_2^2\right|, \quad (2)$$

taking the minimal value $C = 0$ for a pair of co-polarized photons and the maximal value $C = 1$ for a pair of orthogonally polarized photons.

To analyze the polarization state of the generated pairs, we apply a simplified version of the two-photon polarization tomography [24], which enables the reconstruction of the state in Eq. (1) or, for a mixed state, of the corresponding density matrix ρ. The procedure is similar to the Stokes measurements on single photons [19], but involves coincidence registration. In each beam splitter output port, we independently select different polarization states and measure the rate of coincidences. Since the density matrix ρ of the two-photon polarization state has a dimension of $n = 3$, we require $n^2 = 9$ measurements (including one extra measurement for normalization) of the coincidence count rate to fully reconstruct the state [25], see Supplement 1. In the more general case of photon pairs generated in two spatial modes, the dimension of the reduced density matrix is 4, and, as a consequence, 16 measurements are required for quantum tomography [24].

The reconstructed density matrices ρ of photon pairs generated by the H- and V-polarized pump before the beam splitter are shown in Fig. 2(a). For the H-polarized pump, the two-photon

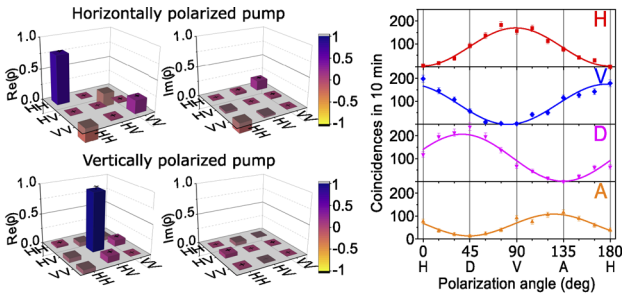

Fig. 2. (a) Real and imaginary parts of the density matrix ρ of the photon pairs generated by the H- (V-) polarized pump and (b) the number of coincidences versus the linear polarization angle selected in arm A for the V-polarized pump, i.e., orthogonally polarized photons. In arm B, we select linearly polarized states: horizontal (H), vertical (V), diagonal (D), anti-diagonal (A). Solid lines show the theoretical dependence for polarization-entangled photons.

polarization state is a superposition of the horizontally and vertically polarized pairs with different weights: $|C_1|^2 = 0.79 \pm 0.02$, $|C_2|^2 = 0$, and $|C_3|^2 = 0.21 \pm 0.02$. Since $|C_1|^2 \gg |C_3|^2$, two photons within a pair are almost co-polarized horizontally. In contrast, pairs generated with the V-polarized pump contain orthogonally (HV) polarized photons: $|C_1|^2 = 0.03 \pm 0.01$, $|C_2|^2 = 0.97 \pm 0.06$, and $|C_3|^2 = 0$. These results demonstrate a vast tunability of the two-photon polarization state, which is not achievable with a single bulk SPDC source and requires additional linear elements [24].

Moreover, by changing the polarization of the pump, we also tune the degree of polarization entanglement. In the case of an H-polarized pump, Eq. (2) yields the concurrence $C = 0.4 \pm 0.03$, i.e., photons within a pair are almost disentangled. For the HV photon pairs, obtained from a V-polarized pump, the degree of entanglement is maximal, $C = 0.98 \pm 0.02$. Notably, this tunability is impossible with standard linear polarization elements, which maintain the degree of entanglement and can modify it only through lossy transformations [9].

We further demonstrate the polarization entanglement of photon pairs generated with the V-polarized pump by measuring the number of coincidences for different orientations of the analyzers. The analyzer in arm B is fixed at one of the basic polarization states, horizontal (H), vertical (V), diagonal (D), or anti-diagonal (A). The analyzer in arm A is then selecting linear polarization, rotated from 0° to 180° [Fig. 2(b)]. A visibility of 96% witnesses strong polarization entanglement.

By splitting photon pairs generated with the V-polarized pump with the non-polarizing beam splitter, we create the Bell state $|\Psi^{(+)}\rangle$ (see Supplement 1) and use it to test the Bell inequality in the Clauser–Horne–Shimony–Holt form [26],

$$F \equiv \frac{1}{2}|\langle ab + a'b + ab' - a'b'\rangle| \le 1. \quad (3)$$

We choose the binary variables a, a', b, $b' = \pm 1$ for photons in arms A and B as their Stokes operators S_1^A, $-S_2^A$, $\frac{1}{\sqrt{2}}(S_1^B + S_2^B)$, and $\frac{1}{\sqrt{2}}(S_1^B - S_2^B)$, respectively [27]. By measuring simultaneously the Stokes observables of photons A, B in the two output ports of the beam splitter and calculating the left-hand side of the inequality in Eq. (3), we obtain $F = 1.36 \pm 0.07$, which violates the Bell inequality by five standard deviations.

Remarkably, generation of polarization-entangled photon pairs with high purity does not require any additional elements erasing the distinguishability between pairs of different polarization states, in contrast to bulk sources [28]. For orthogonally polarized photons, we obtain the purity $Tr(\rho^2) = 1.0 \pm 0.1$. The indistinguishability stems from the isotropic linear optical properties of GaP. A similar feature is expected in other nonlinear crystals with zinc blende structure like GaAs or InAs [18].

As we see in Fig. 2(b), H-V photon pairs generated by the V-polarized pump result in no coincidences if the polarization analyzers select the D-A polarization states. This is the polarization version of the HOM effect [29,30] and another manifestation of polarization entanglement. Destructive quantum interference leads to the absence of coincidences for D-A polarization output states. In contrast, when the analyzers are both oriented diagonally (D-D) or anti-diagonally (A-A), the rate of coincidences is maximal due to the constructive interference. This behavior is similar to the "standard" version of the HOM effect: two photons arriving from different input ports of a beam splitter (here, from orthogonal polarization modes H,V) are both directed into one of the output ports (here, into polarization mode D or A).

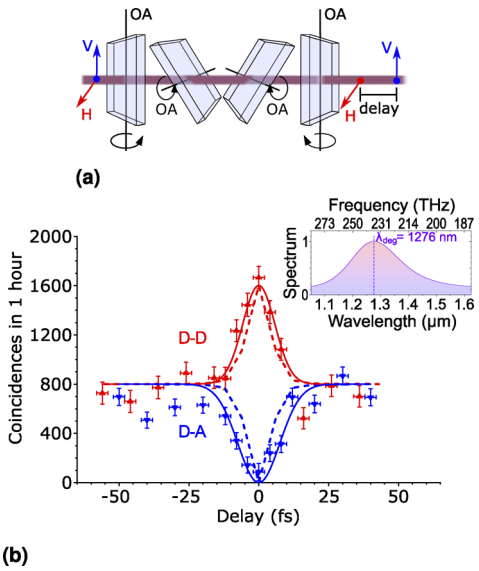

Fig. 3. (a) Delay line for the HOM experiment: four calcite plates whose birefringence introduces a delay between orthogonally polarized photons. The delay is varied by tilting the plates around their optic axes (OA). (b) HOM dip (blue) and peak (red), measured (points) and calculated based on the Fourier transform of the spectrum in the inset (dashed lines). Solid lines show the Gaussian fit of the experimental data.

By introducing a time delay between the photons of a pair, one observes a dip in the case of destructive interference and a peak in the case of constructive interference. The shape of the dip or peak is obtained by Fourier-transforming the SPDC spectrum and scaling the result down in time by a factor of "2" [31]. Here, the spectrum is ultrabroad due to the tiny thickness of the sample, resulting in a HOM peak or dip approximately 10-fs wide. The inset of Fig. 3(b) shows the calculated spectrum, with the etalon effect taken into account [32,33]. Despite the reduction due to the etalon effect [14], the spectral width is still as large as 50 THz, which should lead to the HOM dip and peak of width approximately 10 fs [dashed lines in Fig. 3(b)].

To measure the HOM effect, we introduce the time delay between orthogonally polarized photons before the beam splitter by means of four 5-mm-thick calcite crystal plates [Fig. 3(a)], with the optic axes vertical for two and horizontal for the other two plates. Tilting the plates around their optic axes changes their effective thickness. Due to the birefringence of calcite, the optical path for the H- and V-polarized photons is different, which leads to a delay between them depending on the tilt angle of a plate. The zero delay is achieved when two orthogonally oriented crystal plates are tilted by the same angle. To compensate for the transverse displacement of the beam, we put a mirrored scheme with another two plates. By rotating the inner (outer) pair of plates, we achieve negative (positive) delays between two orthogonally polarized photons.

The results [Fig. 3(b)] show a dip of coincidences at zero delay when the analyzers select orthogonal polarization states, D-A, and a peak when they select the same polarization states, D-D. At large time delays, quantum interference disappears because single-photon wave packets do not overlap in time. The widths of the dip and the peak are 15 ± 2 fs and 12 ± 2 fs, respectively, which is somewhat larger than the width predicted from the calculated spectrum (10 fs). This is because the two-photon

spectrum is additionally narrowed by the spectrally dependent efficiency of the detectors.

In conclusion, we show that the relaxed phase matching for SPDC in an ultrathin nonlinear film leads to the unprecedented polarization tunability of the produced photon pairs. By simply adjusting the pump polarization, we drastically tune the two-photon polarization state and change it from maximally polarization entangled to almost disentangled. This tunability provides enormous freedom in photon pair polarization engineering, impossible in conventional systems without introducing losses. Easy tuning of the polarization entanglement is useful for various applications of quantum technologies: quantum key distribution [34], teleportation [35], and Bell inequality tests [36].

To verify the high degree of polarization entanglement of one of the states, we experimentally violate the Bell inequality by five standard deviations. This is the first observation of polarization-entangled photons from ultrathin nonlinear films. The state is of high purity even without linear optical polarization compensators, unavoidable with bulk SPDC sources.

Polarization entanglement comes in combination with an ultrabroad frequency spectrum, an extremely high degree of time/frequency entanglement [13], and ultra-narrow time correlations. Accordingly, we observe a very narrow (12–15 fs) polarization HOM effect, which can be used for polarization-sensitive quantum-optical coherence tomography [37]. We note that the width of the HOM dip and peak can be further reduced by improving the detection setup.

The combination of polarization with other degrees of freedom enables achieving hyperentanglement, which allows superdense coding, considerably increasing the information capacity of two-photon states [38]. So far, SPDC in ultrathin films resulted in photon pairs with huge entanglement in frequency [13] and momentum [16]. Now, we complement this set with the polarization degree of freedom. It can be further extended by considering entanglement in orbital-angular momentum (OAM) [39].

Funding. Deutsche Forschungsgemeinschaft (429529648 – TRR 306 QuCoLiMa).

Acknowledgments. We thank H. Zhang, A. P. Anthur, and L. A. Krivitsky for providing the sample and A. V. Rasputnyi for the help at the initial stage of the experiment. V.S. and T.S.C. are part of the Max Planck School of Photonics supported by BMBF, Max Planck Society, and Fraunhofer Society.

Disclosures. The authors declare no conflicts of interest.

Data availability. Data underlying the results presented in this paper are available from the authors upon reasonable request.

Supplemental document. See Supplement 1 for supporting content.

REFERENCES

1. N. Yu and F. Capasso, Nat. Mater. **13**, 139 (2014).
2. W. T. Chen and F. Capasso, Appl. Phys. Lett. **118**, 100503 (2021).
3. Yu. Wang, K. D. Jöns, and Zh. Sun, Appl. Phys. Rev. **8**, 011314 (2021).
4. A. S. Solntsev, G. S. Agarwal, and Yu. S. Kivshar, Nat. Photonics **15**, 327 (2021).
5. M. Toth and I. Aharonovich, Annu. Rev. Phys. Chem. **70**, 123 (2019).
6. K. Wang, J. G. Titchener, S. S. Kruk, L. Xu, H.-P. Chung, M. Parry, I. I. Kravchenko, Y.-H. Chen, A. S. Solntsev, Yu. S. Kivshar, D. N. Neshev, and A. A. Sukhorukov, Science **361**, 1104 (2018).
7. L. Li, Z. Liu, X. Ren, S. Wang, V.-C. Su, M.-K. Chen, C. H. Chu, H. Y. Kuo, B. Liu, W. Zang, G. Guo, L. Zhang, Z. Wang, S. Zhu, and D. P. Tsai, Science **368**, 1487 (2020).
8. Q. Li, W. Bao, Z. Nie, Y. Xia, Y. Xue, Y. Wang, S. Yang, and X. Zhang, Nat. Photonics **15**, 267 (2021).
9. S. Lung, K. Wang, K. Z. Kamali, J. Zhang, M. Rahmani, D. N. Neshev, and A. A. Sukhorukov, ACS Photonics **7**, 3015 (2020).
10. F. Xu, X. Ma, Q. Zhang, H. Lo, and J. Pan, Rev. Mod. Phys. **92**, 025002 (2020).
11. H.-S. Zhong, H. Wang, Y.-H. Deng, M.-C. Chen, L.-C. Peng, Y.-H. Luo, J. Qin, D. Wu, X. Ding, Y. Hu, P. Hu, X.-Y. Yang, W.-J. Zhang, H. Li, Y. Li, X. Jiang, L. Gan, G. Yang, L. You, Z. Wang, L. Li, N.-L. Liu, C.-Y. Lu, and J.-W. Pan, Science **370**, 1460 (2020).
12. K. F. Lee, Y. Tian, H. Yang, K. Mustonen, A. Martinez, Q. Dai, E. I. Kauppinen, J. Malowicki, P. Kumar, and Z. Sun, Adv. Mater. **29**, 1605978 (2017).
13. C. Okoth, A. Cavanna, T. Santiago-Cruz, and M. V. Chekhova, Phys. Rev. Lett. **123**, 263602 (2019).
14. T. Santiago-Cruz, V. Sultanov, H. Zhang, L. A. Krivitsky, and M. V. Chekhova, Opt. Lett. **46**, 653 (2021).
15. N. M. Hanh Duong, A. Maeder, G. Saerens, F. Kaufmann, and R. Grange, in *2021 Conference on Lasers and Electro-Optics Europe & European Quantum Electronics Conference (CLEO/Europe-EQEC)* (2021), p. 1.
16. C. Okoth, E. Kovlakov, F. Bönsel, A. Cavanna, S. Straupe, S. P. Kulik, and M. V. Chekhova, Phys. Rev. A **101**, 011801 (2020).
17. A. P. Anthur, H. Zhang, Yu. Akimov, J. R. Ong, D. Kalashnikov, A. I. Kuznetsov, and L. Krivitsky, Opt. Express **29**, 10307 (2021).
18. R. W. Boyd, *Nonlinear optics* (Academic press, San Diego, CA, 2003).
19. M. Chekhova and P. Banzer, *Polarization of Light: In Classical, Quantum, and Nonlinear Optics* (De Gruyter, Berlin, Boston, 2021).
20. R. Hanbury Brown and R. Q. Twiss, Nature **177**, 27 (1956).
21. A. V. Burlakov, M. V. Chekhova, O. A. Karabutova, D. N. Klyshko, and S. P. Kulik, Phys. Rev. A **60**, R4209 (1999).
22. W. K. Wootters, Phys. Rev. Lett. **80**, 2245 (1998).
23. M. V. Fedorov and N. I. Miklin, Contemp. Phys. **55**, 94 (2014).
24. A. G. White, D. F. V. James, P. H. Eberhard, and P. G. Kwiat, Phys. Rev. Lett. **83**, 3103 (1999).
25. A. V. Burlakov, L. A. Krivitskii, S. P. Kulik, G. A. Maslennikov, and M. V. Chekhova, Opt. Spectrosc. **94**, 684 (2003).
26. J. F. Clauser, M. A. Horne, A. Shimony, and R. A. Holt, Phys. Rev. Lett. **23**, 880 (1969).
27. D. N. Klyshko, Phys.-Usp. **41**, 885 (1998).
28. P. G. Kwiat, K. Mattle, H. Weinfurter, A. Zeilinger, A. V. Sergienko, and Y. Shih, Phys. Rev. Lett. **75**, 4337 (1995).
29. C. K. Hong, Z. Y. Ou, and L. Mandel, Phys. Rev. Lett. **59**, 2044 (1987).
30. M. H. Rubin, D. N. Klyshko, Y. H. Shih, and A. V. Sergienko, Phys. Rev. A **50**, 5122 (1994).
31. A. V. Burlakov, M. V. Chekhova, O. A. Karabutova, and S. P. Kulik, Phys. Rev. A **64**, 041803 (2001).
32. G. Kh. Kitaeva and A. N. Penin, J. Exp. Theor. Phys. **98**, 272 (2004).
33. Y. Jeronimo-Moreno, S. Rodriguez-Benavides, and A. B. U'Ren, Laser Phys. **20**, 1221 (2010).
34. P. Xue, C.-F. Li, and G.-C. Guo, Phys. Rev. A **64**, 032305 (2001).
35. J. Modławska and A. Grudka, Phys. Rev. Lett. **100**, 110503 (2008).
36. M. Giustina, M. A. M. Versteegh, S. Wengerowsky, J. Handsteiner, A. Hochrainer, K. Phelan, F. Steinlechner, J. Kofler, J.-Å. Larsson, C. Abellán, W. Amaya, V. Pruneri, M. W. Mitchell, J. Beyer, T. Gerrits, A. E. Lita, L. K. Shalm, S. W. Nam, T. Scheidl, R. Ursin, B. Wittmann, and A. Zeilinger, Phys. Rev. Lett. **115**, 250401 (2015).
37. M. C. Booth, G. D. Giuseppe, B. E. A. Saleh, A. V. Sergienko, and M. C. Teich, Phys. Rev. A **69**, 043815 (2004).
38. T. M. Graham, H. J. Bernstein, T.-C. Wei, M. Junge, and P. G Kwiat, Nat. Commun. **6**, 7185 (2015).
39. C. Xu, S. Huang, Q. Yu, D. Wei, P. Chen, S. Nie, Y. Zhang, and M. Xiao, Phys. Rev. A **104**, 063716 (2021).